

PAPER • OPEN ACCESS

SYLOS lasers – the frontier of few-cycle, multi-TW, kHz lasers for ultrafast applications at extreme light infrastructure attosecond light pulse source

To cite this article: S Toth *et al* 2020 *J. Phys. Photonics* **2** 045003

View the [article online](#) for updates and enhancements.



PAPER

OPEN ACCESS


RECEIVED
11 June 2020ACCEPTED FOR PUBLICATION
24 June 2020PUBLISHED
24 July 2020

Original content from this work may be used under the terms of the [Creative Commons Attribution 4.0 licence](#).

Any further distribution of this work must maintain attribution to the author(s) and the title of the work, journal citation and DOI.



SYLOS lasers – the frontier of few-cycle, multi-TW, kHz lasers for ultrafast applications at extreme light infrastructure attosecond light pulse source

S Toth¹ , T Stanislaukas², I Balciunas², R Budriunas^{2,3}, J Adamonis⁴, R Danilevicius⁴, K Viskontas⁴, D Lengvinas⁴, G Veitas², D Gadonas², A Varanavičius³, J Csontos¹, T Somoskoi¹, L Toth¹, A Borzsonyi¹ and K Osvay^{5,6}

¹ ELI-ALPS, ELI-HU Non-Profit Ltd., Wolfgang Sandner u. 3, H-6728, Szeged, Hungary

² Light Conversion Ltd., Keramiku str. 2b, LT-10233, Vilnius, Lithuania

³ Laser Research Center, Vilnius University, Saulėtekio ave. 10, LT-10223, Vilnius, Lithuania

⁴ EKSPALA UAB, Savanoriu Ave 237, LT-02300, Vilnius, Lithuania

⁵ Department of Optics and Quantum Electronics, University of Szeged, Dóm tér 9, 6720, Szeged, Hungary

⁶ Institute for Applications of High Intensity Lasers in Nuclear Physics, University of Szeged, Dugonics ter 13, 6720, Szeged, Hungary

E-mail: szabolcs.toth@eli-alps.hu

Keywords: ultrafast lasers, attosecond physics, optical parametric amplifiers

Abstract

The extreme light infrastructure attosecond light pulse source offers beamtime for users of various attosecond and particle sources driven by versatile laser systems. Here we report on the state of the art of a few-cycle, multi-TW, 1kHz repetition rate laser system, now fully operational in the facility. The system is based on four stages of optical parametric amplifiers (OPAs) pumped by a total of 320mJ, 80ps frequency-doubled Nd:YAG laser pulses. All OPA stages utilize double crystal configuration, which design has been also confirmed by model calculations. The 1kHz SYLOS 2 system produces 32mJ laser pulses around a central wavelength of 891nm with 6.6fs (<2.3 optical cycles) pulse duration exceeding the peak power of 4.8 TW on a daily basis. The recorded best pulse duration is 6.3fs, which corresponds to 2.12 cycles and 5.1 TW peak power. During long-term (24h) performance tests, energy stability of 1.2%, carrier-envelope phase (CEP) stability of 210mrad, and pointing stability of 0.4 μ rad were demonstrated, while the Strehl ratio of the beam is kept above 0.75. In order to help the alignment of all the different experiments at the facility and to reduce the workload on SYLOS 2 system, a second laser system has been developed. The so-called SYLOS Experimental Alignment (SEA) laser mimicks the performance of the SYLOS 2 laser, but at a repetition rate two orders of magnitude lower and without CEP-stabilization. The three single-crystal OPA stages of the SEA laser provide 42mJ pulse energy for the users, while having energy stability of 0.87% and sub-13fs pulse duration at a repetition rate ranging from a single shot up to 10Hz.

1. Introduction

Laser systems producing high peak power, carrier-envelope phase (CEP)-stable, few-cycle pulses are indispensable tools for the generation of short, isolated attosecond pulses [1–5] and for electron acceleration [6–10]. Terrawatt and even petawatt level pulses can be generated in Ti:Sapphire based chirped pulse amplification (CPA) systems, however, special techniques must be applied to overcome the barrier of gain narrowing [11–14], which limits the achievable pulse duration around 40fs. One way to reach few-cycle duration at terawatt level is post-compression of these robust Ti:Sapphire CPA systems. This way, pulses as short as 4fs are generated using self-phase modulation (SPM) in hollow-core fibres [15, 16]. Post-compression techniques are in general scalable in average power [17, 18], however pulse energy is limited to a few millijoules.

Another method to produce TW-level, few-cycle pulses is optical parametric chirped pulse amplification (OPCPA), as it allows the amplification of large signal bandwidth. Low crystal absorption ensures the average power scalability and furthermore, the parametric process is phase preserving [19]. These advantageous properties of the technique and the maturing of the $1\mu\text{m}$ pump laser technology [20–28] induced a rapid growth of OPCPA systems producing sub-10 fs, millijoule-level pulses [29–38].

Some of these systems operate at a repetition rate of few tens of Hz and produce TW-level, few-cycle pulses. These OPCPAs are typically driven by flash-lamp pumped Nd:YAG lasers [29–31]. A good example of these systems is the OPCPA system described in [29], which is pumped by the second- and third-harmonic of a flash-lamp pumped Nd:YAG laser and produces 75mJ 4.5fs (16 TW) pulses at 10Hz repetition rate. Similarly, 130mJ, 7.9fs (16 TW) [30], and 15mJ, 7.6fs (2 TW) [31] pulses were generated at 10Hz and 30Hz repetition rates respectively. The system described in [32] is also operating at 10Hz, but it is driven by the sub-picosecond pulses of diode-pumped Yb:YAG CPA system and was producing 7fs, 42mJ (6 TW) pulses.

There are also many notable systems which operate in the kHz repetition rate range and produce sub-TW few-cycle pulses. It was reported that 5.5fs, 2.7mJ pulses were produced in a BBO based OPCPA which was pumped by the second-harmonic of a 1kHz Ti:Sapphire CPA system [33]. In the OPCPA, reported in [34], the signal spectrum was multiplexed in different amplifier channels, which were pumped by second harmonics of picosecond pump pulses from an Yb:YAG thin-disk laser. This system was capable of delivering a 4.3fs bandwidth; however compression was not optimized, and sub-10fs pulses were obtained [34]. In [35] 7fs, 1.8mJ pulses were delivered at 6kHz repetition rate from an OPCPA, which was also driven by an Yb-doped thin-disk laser. It is also worth mentioning the system described in [36], which produces 0.19mJ, 7fs pulses at 100kHz repetition rate.

The single cycle laser (SYLOS) in the extreme light infrastructure attosecond light pulse source (ELI-ALPS) aims to provide CEP-stabilized, near single-cycle pulses with 15 TW peak power at 1kHz repetition rate. In the first development phase, which concluded in 2017, SYLOS1 was successfully delivered with output parameters of 5.5 TW peak power, sub-9fs pulse duration and 220mrad CEP-stability at 1kHz repetition rate [37], becoming the first TW-class few-cycle OPCPA system at kHz repetition rate.

During the second development phase called SYLOS 2, the goal was to develop SYLOS 1 towards a pulse duration close to two cycles, while keeping the peak power at the same level. This was achieved by the direct amplification of broadband seed pulses in a noncollinear OPCPA, where the spectrum was multiplexed [34, 38] using LBO and BBO crystal pairs in different orientations. This development was supported by extensive numerical simulation of the broadband OPCPA schemes. The optical layout was realized based on these computations. After the experimental finalization of the system, 32mJ pulses were delivered at 1kHz repetition rate with 6.6fs (<2.3 cycle) pulse duration during the long-term tests, however the best value which was demonstrated was 6.3fs (2.17 optical cycles). With these parameters, the SYLOS 2 system occupies a unique position in the parameter space among similar high peak power, few-cycle lasers. It would be possible to shorten pulse duration even more by pumping OPCPAs with combined 2nd and 3rd harmonics [29, 39, 40], but in practice, this is not advisable for a laser system planned for high user demand at kHz repetition rate due to the low resilience of optical components to UV light. On the other hand, pulse duration is considerably shorter than what is achievable with Ti:Sapphire lasers of comparable peak power. Moreover, the attainable output pulse energy is about an order of magnitude higher compared to nonlinear pulse compression techniques.

The SYLOS laser will serve at least five beamlines at ELI-ALPS dedicated for high harmonic generation, electron acceleration and neutron generation, so that it is expected to be in high demand. However, for the alignment and preparation of the secondary sources and the connected experimental end-stations a low repetition rate laser, even at single shot, would be suitable. Hence, a laser system called SYLOS Experimental Alignment (SEA) laser, mimicking the performance of the SYLOS 2 laser has been also produced. SEA laser is able to run from a single shot up to 10Hz repetition rate, and it provides 42mJ, sub-13 fs pulses. This way peak power and bandwidth is similar for the alignment of experimental targets, but the heat load is reduced resulting from high average power.

This paper presents the structures and performance tests of the SYLOS 2 and SEA lasers, together with the numerical study of broadband OPCPA schemes utilized during the current development phase.

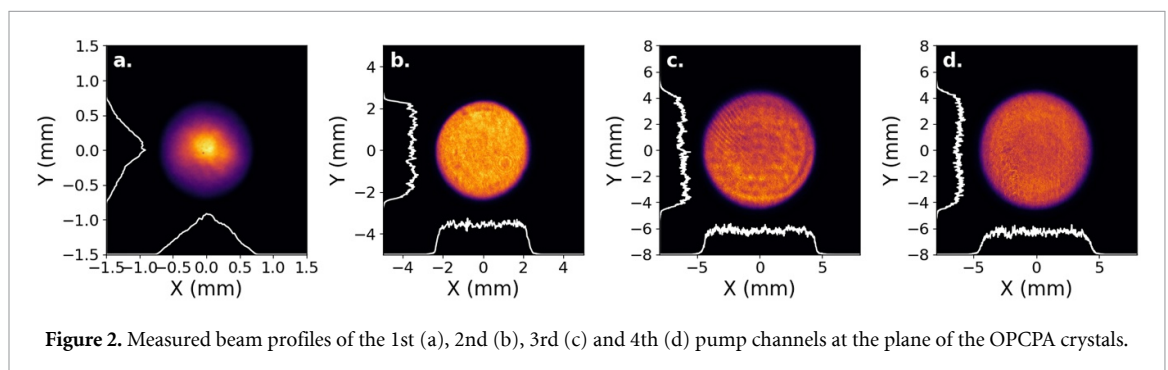
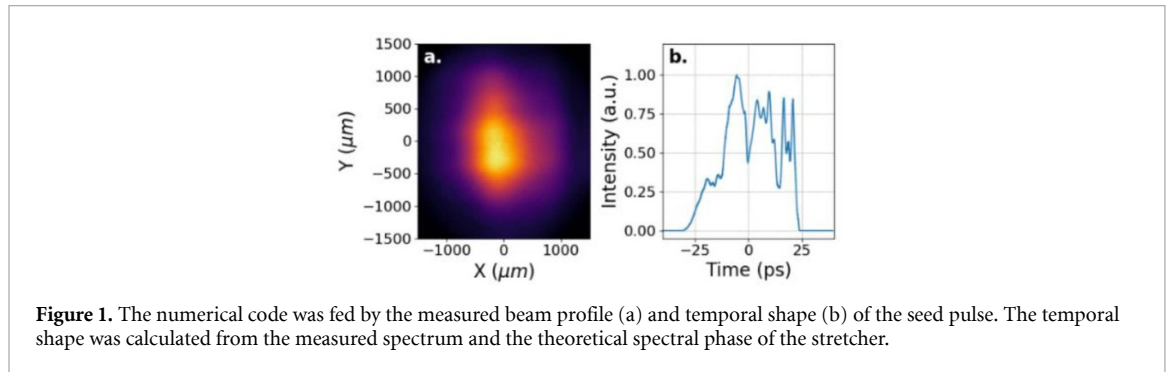
2. Numerical model of broadband OPCPA schemes

2.1. Modelling methods and input parameters

Modelling was carried out using a four-dimensional numerical code for three-wave mixing, which takes into account dispersion, diffraction, birefringence (walk-off), non-collinear propagation and crystal absorption. Furthermore, it utilizes a special algorithm for highly chirped pulses, which relaxes the requirements on temporal grid resolution, making OPCPA modelling possible on a desktop computer [41].

Table 1. Pump parameters.

	OPCPA 1	OPCPA 2	OPCPA 3	OPCPA 4
Energy (mJ)	4	65	105	140
Intensity (GWcm^{-2})	10	3.5	2.7	3.55
Temporal shape	6th order Gaussian	6th order Gaussian	1st order Gaussian	1st order Gaussian
FWHM duration (ps)	120	120	90	90



The seed pulse used for the modelling of OPCPA was constructed from the measured beam profile (figure 1(a)) at the plane of the first amplifier crystal, and from the temporal shape (figure 1(b)), which was calculated from the real spectrum measured after the stretcher and the theoretical spectral phase of the stretcher. The duration of the $1\mu\text{J}$, stretched seed pulse was 50ps, in order to avoid gain narrowing in the last two OPCPA stages, which are pumped by 90ps long 1st order Gaussian pump pulses (table 1.) The spatial shapes of the pump pulses were also taken from actual measurements, which are shown in figure 2., while the temporal shapes were simulated by Gaussian functions. The order of the Gaussian functions and all the other pump parameters of each pump channel are summarized in table 1.

2.2. Broadband phase matching in LBO

In the near-IR spectral range, the two mostly favoured nonlinear crystals are Beta Barium Borate (BBO) and Lithium Triborate (LBO), as they can amplify over a very broad wavelength range when operated in noncollinear geometry. LBO has a lower effective nonlinear coefficient (0.83pmV^{-1}) than BBO (2pmV^{-1}), hence at least twice as long LBO is needed to reach the same efficiency as in BBO. The examination of the spectral gain curves, which are calculated using the undepleted pump approximation [42], revealed that a 12mm thick LBO at 1.1° noncollinear and 12.7° phase-matching angles and at 10GWcm^{-2} pump intensity can amplify a very broad spectral band, supporting 5fs Fourier-limited pulse duration (green curve in figure 3). This result was also verified by numerical simulations using the pump and signal parameters described in the previous section and the crystal parameters mentioned above. Numerical modelling revealed that the spectral gain above $1\mu\text{m}$ is considerably lower than it was predicted by the undepleted pump approximation.

The duration of the pump in the 1st and 2nd OPCPA stages is more than twice longer than the seed pulse duration (table 1), therefore, to reach higher conversion efficiency, the pump after one nonlinear crystal can be re-used in a second one, by using different temporal sections of the pump for amplification. Before the modelling of pump recycling, the signal and pump pulses were numerically relay imaged to the surface of the second crystal, and the signal pulse was delayed by 50ps compared to the pump pulse. In this manner, the 50ps long stretched signal pulse was spatiotemporally overlapped with the undepleted part of the 120ps long pump pulse. According to the results, the signal energy after the 1st crystal is $250\mu\text{J}$, and it can be boosted up

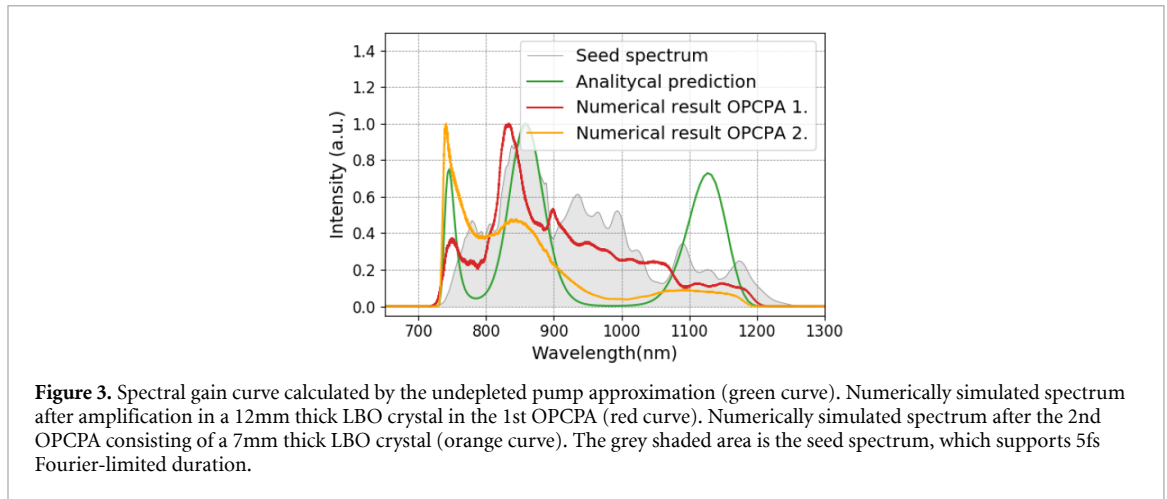
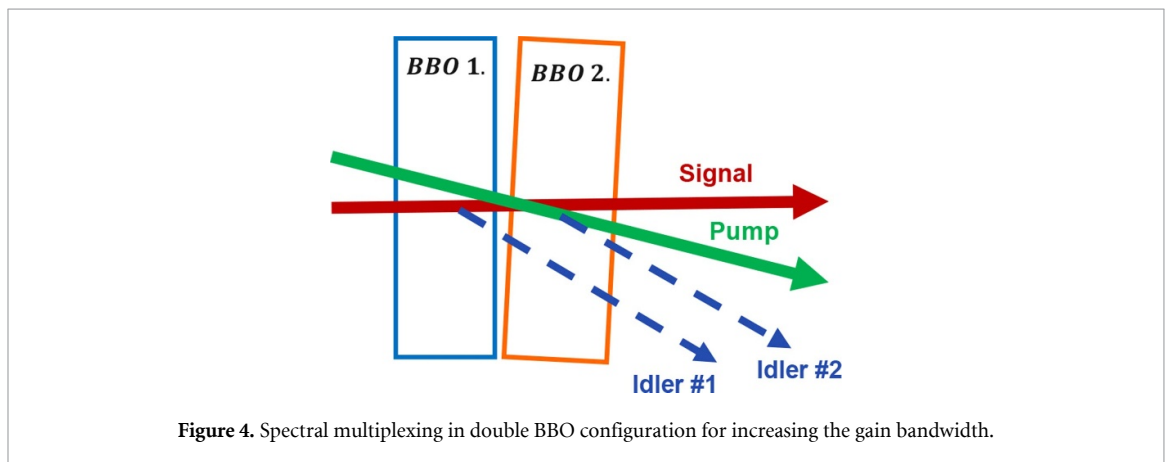


Table 2. Noncollinear and phase-matching angles in the double BBO configuration.

	Config. 1	Config. 2
Noncollinear angle ($^{\circ}$)	1.97	2.23
Phase-matching angle in the 1st BBO ($^{\circ}$)	23.28	23.66
Phase-matching angle in the 2nd BBO ($^{\circ}$)	23.42	23.45



to 450 μ J by adding an extra 4mm thick LBO crystal. The calculated signal spectrum after the first OPCPA stage is plotted in figure 3 (red curve) together with the input signal spectrum (grey shaded area).

In the second OPCPA stage, the calculated signal spectrum after amplification in a 7mm thick LBO crystal is shown in figure 3 (orange curve). According to the simulations, this crystal thickness was enough to deplete the pump pulse. The calculated energy after this stage is 9mJ.

In the subsequent power amplifier stages, where the pump intensity on the crystals is around 3GWcm⁻², the spectral gain at the long wavelength side of the spectrum decreases along with the pump-to-signal conversion efficiency. Therefore, other solutions, such as using different crystals (described in the following sections), had to be explored.

2.3. Spectral multiplexing in double BBO configuration

Spectral multiplexing is an approach, where different parts of the broadband signal are amplified in subsequent crystals with different orientations. In the current case, a compact double BBO arrangement was studied numerically. In this arrangement, two thin BBO crystals are placed very close to each other (figure 4). The noncollinear angle between the signal and pump beams is the same in both crystals, but the phase matching angles are slightly different, as indicated in table 2.

This arrangement is particularly advantageous in case of super-Gaussian beam profiles, as there is no need for an additional image relay system between the two subsequent crystals. This makes the optical setup simple, compact and allows for a broad amplification bandwidth.

The double BBO configuration can be realized in two schemes. In the first scheme (Config. 1 in table 2), the first and second BBOs amplify the central and outer part of the signal spectrum, respectively (figure

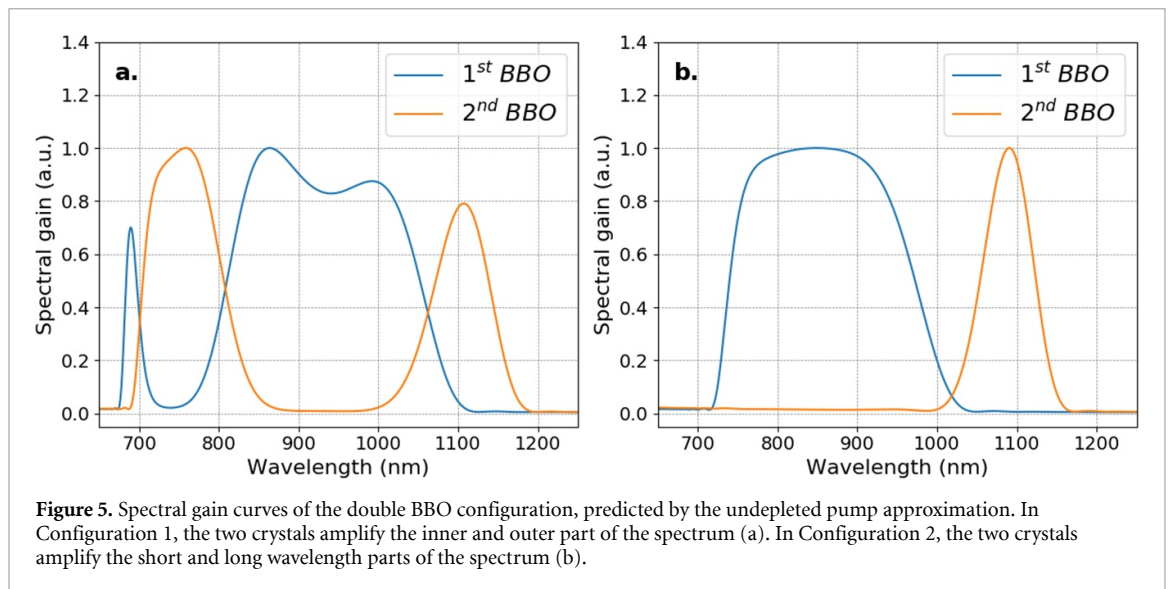


Figure 5. Spectral gain curves of the double BBO configuration, predicted by the undepleted pump approximation. In Configuration 1, the two crystals amplify the inner and outer part of the spectrum (a). In Configuration 2, the two crystals amplify the short and long wavelength parts of the spectrum (b).

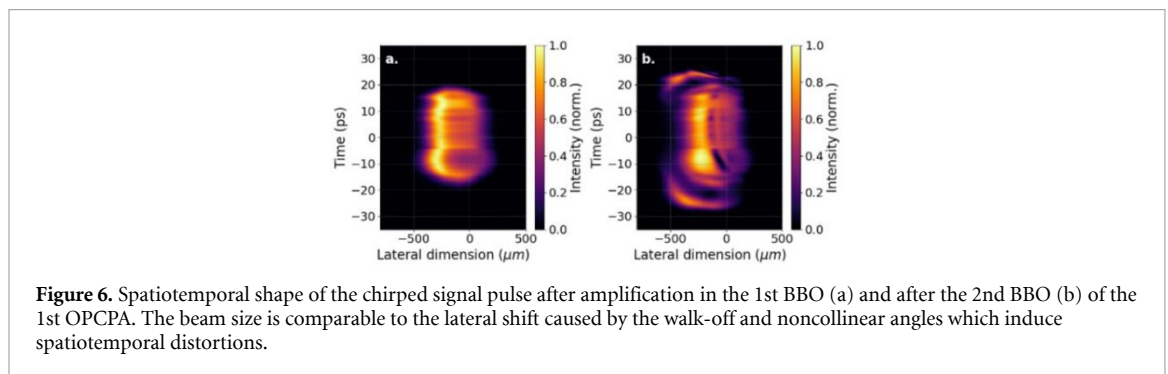


Figure 6. Spatiotemporal shape of the chirped signal pulse after amplification in the 1st BBO (a) and after the 2nd BBO (b) of the 1st OPCPA. The beam size is comparable to the lateral shift caused by the walk-off and noncollinear angles which induce spatiotemporal distortions.

5(a)). In the other configuration (Config. 2 in table 2), the short and long wavelength part of the spectrum is amplified in the first and second crystals (figure 5(b)). The spectral gain curves of the double BBO configuration, which are calculated using the undepleted pump approximation [42], are plotted in figure 5.

During amplification in nonlinear crystals, the pump and signal beams are spatially separated because of the lateral walk-off and the noncollinear angle. When small beams and thick crystals are used, the lateral shift of the pump and signal pulses are comparable to the beam size. In case of the double BBO configuration, this can result in spatio-spectral and spatiotemporal distortions, as the amplification of different spectral parts will occur at different spatial locations. This effect was numerically studied in case of the 1st OPCPA stage, where the beam size is roughly 1mm at FWHM, and the results are shown in figure 6. To obtain good efficiency, the double BBO arrangement must consist of at least two 5mm thick BBO crystals. Figures 6 (a) and (b) show the spatiotemporal shape of the amplified signal pulse after the first and second crystals, respectively. It is visible that the double BBO configuration introduces spatial chirp in case of small beams and thick crystals, even if the noncollinear angle compensates for the walk-off angle.

In case of power amplifiers, where the diameter of the beam is increased to a few millimetres, and thin crystals are used, spatiotemporal distortions are minimal. This is illustrated on the example of the 3rd OPCPA stage, where the pump and signal beam size is roughly 8mm, and the double BBO configuration consists of a 3mm and a 4mm thick BBO crystals (figure 7).

Based on these results, it can be concluded that in case of preamplification stages, where the beam size is small, double-BBO is less favourable than a single LBO crystal for the amplification of two-cycle bandwidth, as it introduces spatiotemporal couplings. In power amplification stages, where the beam size is bigger compared to the crystal thickness, double-BBO is preferred due to the higher conversion efficiency.

The spectral evolution during amplification in the 1st and 2nd BBO crystals of the double BBO configuration is depicted in figures 8(a) and (b), respectively. This figure illustrates that the 1st (figure 8(a)) and 2nd (figure 8(b)) BBO crystals are amplifying the edges and center of the spectrum respectively. The idler which is generated in the 1st BBO is also present in the 2nd crystal, together with the amplified signal and residual pump. Consequently, signal and idler are trying to combine again, however the phase-mismatch is huge. Therefore, they are just weakly interacting and this interaction will result in low magnitude intensity oscillations with small length periods. This is illustrated by figure 8(b) at the edges of the spectrum.

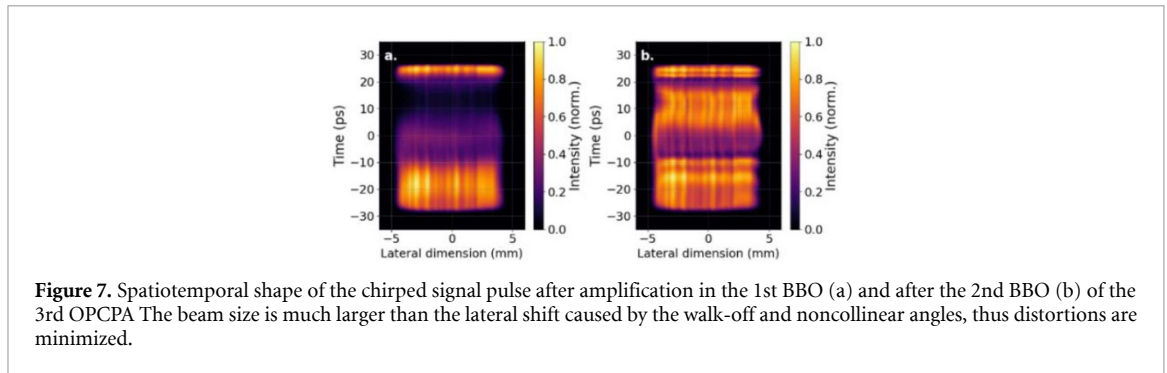


Figure 7. Spatiotemporal shape of the chirped signal pulse after amplification in the 1st BBO (a) and after the 2nd BBO (b) of the 3rd OPCPA. The beam size is much larger than the lateral shift caused by the walk-off and noncollinear angles, thus distortions are minimized.

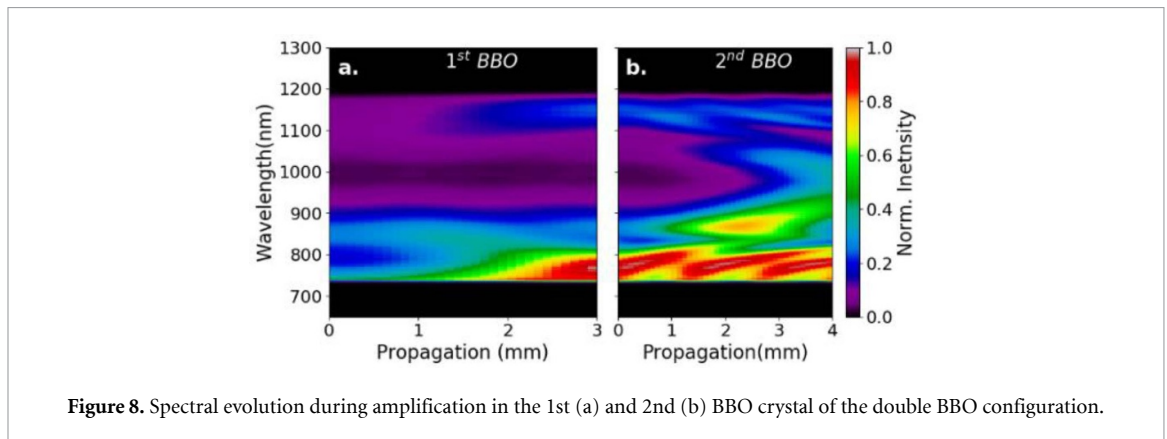


Figure 8. Spectral evolution during amplification in the 1st (a) and 2nd (b) BBO crystal of the double BBO configuration.

Table 3. OPCPA parameters used during modelling.

	OPCPA1	OPCPA2	OPCPA3	OPCPA4
Crystals	LBO+LBO	LBO	Double BBO config. 1.	Double BBO config. 2.
Thickness (mm)	12+4	7	3+4mm	3+3mm
Output energy (mJ)	0.45	9	26	46.8

The other critical point of the double BBO configuration is the behaviour of the spectral phase at the locations, where the gain curve of the two crystals are overlapping. In the case of Configuration 1, the gain curves overlap at around 820nm and 1050nm. To examine this numerically, the spectral phase of the amplified pulse after the 3rd OPCPA was compensated up to the 7th order, and the residual phase was plotted in figure 9 with purple curve. According to this there are small dips where the two gain curves are overlapping, however they are small in magnitude, thus, the amplified pulses should be compressible close to the Fourier-limit. The input and amplified spectra after the 1st and 2nd BBO crystals are also plotted in figure 9, and they support 5fs in the Fourier-limit.

2.4. Numerical simulation of the OPCPA chain

Based on the considerations described in the previous sections, a four-stage OPCPA system was numerically simulated to predict the output energy and spectrum. The OPCPA parameters are summarized in table 3.

According to the numerical results, after the 4th OPCPA stage, a pulse energy of 46.8mJ is predicted. The spectrum after the last OPCPA is plotted in figure 10(a). The Fourier-limited duration calculated from the spectrum is 5fs. The compressibility of the spectrum was simulated by compensating the phase up to the 7th order, which yielded 5.5fs compressed pulse duration and 4.9 TW peak power (figure 10.). Note that during the calculation of the peak power, the pulse energy was multiplied by 0.83, which is the transmission of the compressor. These parameters are very close to the experimentally measured results, which are described in the following section.

3. SYLOS 2 laser

3.1. Description of the system

A schematic drawing of the OPCPA system is presented in figure 11. The starting point for the system is a broadband mode-locked Yb:KGW oscillator, which is used to seed two laser amplifiers: a femtosecond Yb:KGW regenerative amplifier (Pharos, Light Conversion), which is used to generate and preamplify the

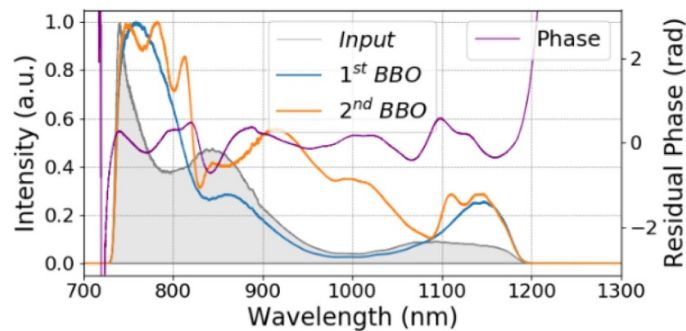


Figure 9. Input signal spectrum for the 3rd OPCPA stage (grey shaded area), spectrum after the 1st BBO (blue curve) and after the 2nd BBO (orange curve) crystals. The residual spectral phase (purple curve, right y-axis) is free from fast oscillations, which suggests that the amplified pulses are compressible close to the Fourier-limit (5 fs).

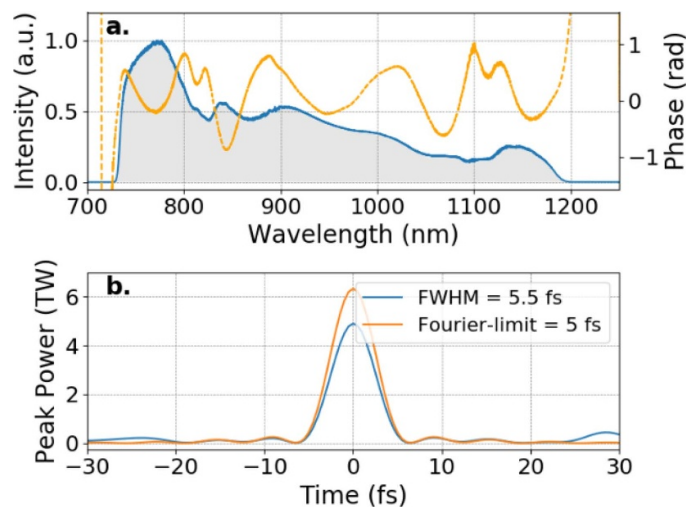


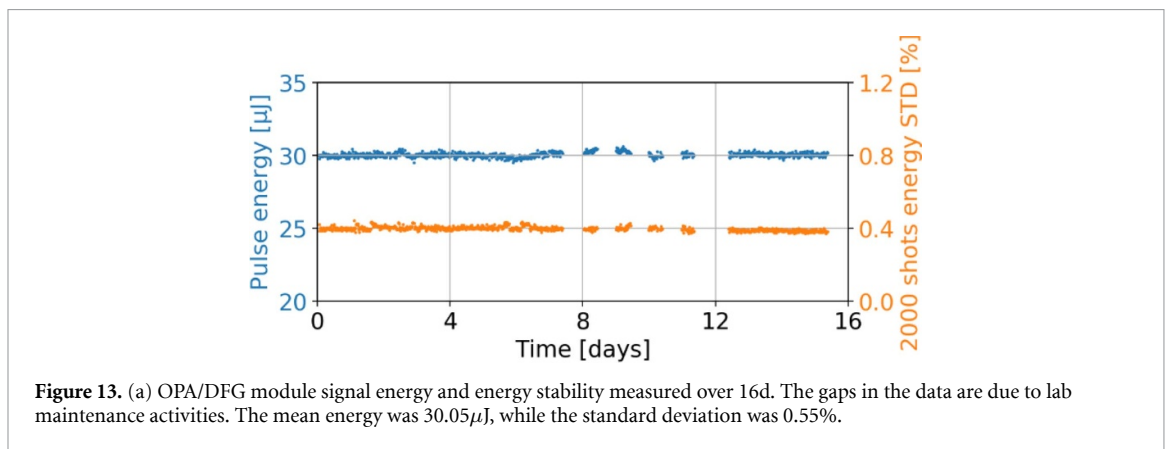
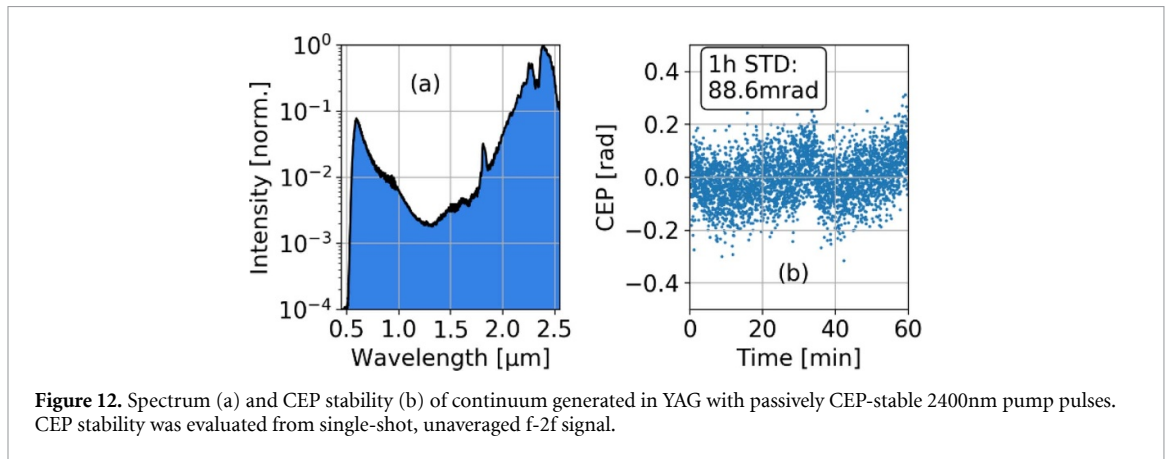
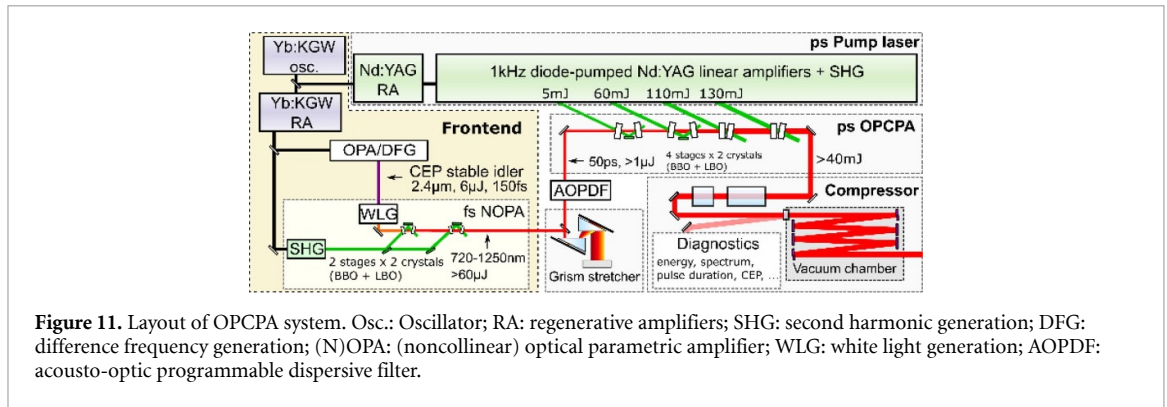
Figure 10. (a) Predicted output spectrum (grey shaded area under the blue curve) and residual spectral phase (orange curve). (b) Fourier-limited (orange curve) and compressed (blue curve) pulse shapes after compensating the spectral phase up to the 7th order.

ultrabroadband, CEP-stable seed pulses, and a picosecond amplifier chain based on Nd:YAG (Ekspla), delivering high energy pump pulses for the chirped pulse optical parametric amplifier (OPA) stages.

The frontend of the system applies passive CEP stabilization scheme based on difference frequency generation (DFG [43]). About $150\mu\text{J}$ of the total 1.5mJ output of the Yb:KGW amplifier is sent to drive an OPA (OPA/DFG in figure 11) to produce a passively CEP-stabilized idler wave. The frontend design has been slightly modified compared to SYLOS 1 [37] in order to support the increased bandwidth of the seed pulses. Typically, the OPA is tuned such way, that the wavelength of the idler is 2400nm , and the pulse duration is about 150fs . Roughly $6\mu\text{J}$ of the total $\sim 15\mu\text{J}$ idler energy is used to generate white light in a YAG crystal, which serves as the broadband, CEP-stable seed for the following OPCPA stages. The spectrum of this CEP-stable continuum is shown in figure 12(a), while a 1h measurement of its CEP stability is shown in figure 12(b). The overall STD is 88.6mrad , including a still notable contribution of slow drift.

Since white light generation is a highly nonlinear process, the stability and reproducibility of the OPA output are critically important for the consistent day-to-day operation of the whole system. To achieve stability and reproducibility adequate for this purpose, the OPA setup is built in a compact enclosure mounted directly on the laser assembly to minimize the influence of day-to-day beam drifts and other disturbances. This allows us to run the OPA/DFG module for extended periods without any adjustments, while maintaining highly consistent output parameters. For illustration purposes, a measurement of long-term pulse energy stability of the signal beam of the OPA/DFG module is shown in figure 13. The compact mechanical design of the OPA and the excellent shot-to-shot energy stability combined with the power stability of the Yb:KGW laser (typically $<0.1\%$ RMS) facilitate the passive CEP-stability of the idler, as already shown in figure 12(b).

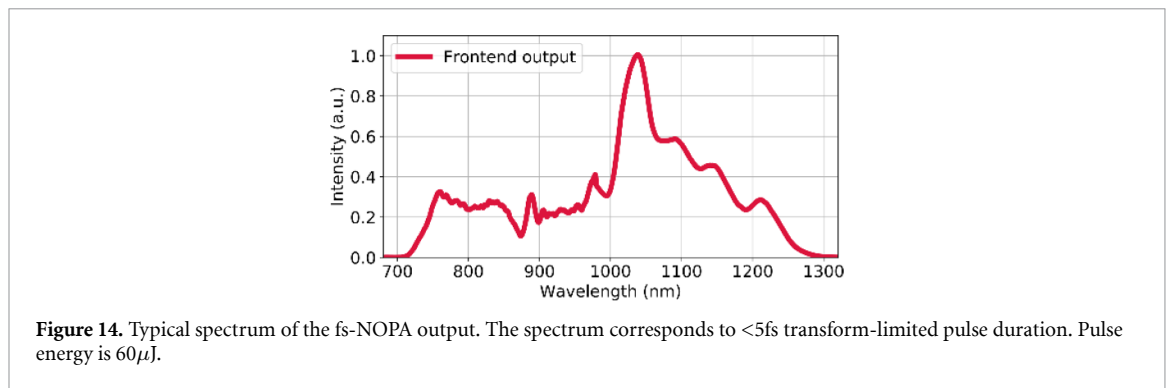
The larger part (1.35mJ) of the Yb:KGW laser pulse energy is frequency doubled and is used for pumping two noncollinear OPA stages, in which the CEP-stable continuum is amplified to $60\mu\text{J}$. Both stages are based



on multiplexed LBO and BBO crystals. When pumped in the femtosecond regime, the multi-crystal, spectrally multiplexed NOPA can amplify bandwidths supporting pulses as short as 1.3 optical cycles. However, in this case, the NOPA is adjusted to maximize the energy content in the spectral range coinciding with the narrower amplification band of the OPCPA stages pumped with picosecond 532nm pulses. The final output spectrum of the frontend is shown in figure 14.

Besides the broad bandwidth and CEP-stability, the design of the frontend is also advantageous in terms of pulse contrast. As the seed is generated by 2400nm pump pulses, any spontaneous amplified emission from the seed laser or parametric fluorescence from the OPA/DFG module used for CEP stabilization is removed with long-pass spectral filters before white light generation, making the white light seed pulses truly background-free. Furthermore, the parametric fluorescence (PSF) originating in the femtosecond-pumped NOPA is contained within a ~ 500 fs window defined by the pump pulse. Furthermore, this PSF is inevitably amplified together with the seed pulses, it is recompressed to a similar duration at the output of the system, and therefore does not produce a long pedestal which could be harmful to many experiments.

The stretching strategy of the OPCPA system was based on the choice of compressor. In order to avoid the temporal contrast and throughput issues with conventional grating compressors, bulk glasses and positively chirped mirrors were selected. The stretcher was designed to pre-compensate for the combined

**Table 4.** Summary of parameters of OPCPA stages.

Stage #	Crystal 1	Crystal 2	Pump intensity (GWcm^{-2})	Efficiency (pump-to-signal conversion)	Amplified signal energy (mJ)
	(Seed)		—	—	0.001
1	LBO 10mm	LBO 12mm	~ 10	7.1%	0.32
2	LBO 8mm	BBO 6mm	~ 3.5	7.2%	5
3	BBO 6mm	BBO 5mm	~ 2.7	11.4%	17
4	BBO 3mm	BBO 4mm	~ 3.5	16.4%	40
	Compressor			83%	32

chirp profile of the amplifiers and the compressor. The large bandwidth requires compensation at least up to the third order, which is possible with a combination of gratings and prisms, in the so-called grism arrangement [44]. The preamplified seed pulses are sent to the grism stretcher, where they are stretched to $\sim 50\text{ps}$. An acousto-optic programmable dispersive filter (AOPDF) is used for controlling high order dispersion and providing slow-loop feedback for the CEP. The combined transmission of the grism pair and the AOPDF is just over 1%, which leaves about $1\mu\text{J}$ of seed energy for the chirped pulse amplification stages.

The picosecond pump laser has not been modified since the previous iteration of the system. It is described in detail in [37], therefore, only a very brief description is given here. The pump laser is based on diode-pumped Nd:YAG laser medium. After spectral filtering, the initial seed pulses from the Yb:KGW oscillator are amplified to $\sim 1\text{mJ}$ in a Nd:YAG. The beam is then split several times, and further amplification is carried out in five amplification chains consisting of regenerative amplifiers and double-passed side-pumped linear amplifiers, producing a total energy of 0.5J at 1064nm . Special waveplates are used in selected points in the amplifier chains to efficiently convert Gaussian beams from regenerative amplifiers into smooth hyper-Gaussian beams to extract maximum energy from the laser rods. The beams are combined in multiple second harmonic generators to produce a total of 4 outputs at 532nm . The shot-to-shot energy stability of all outputs is $\sim 0.5\%$ RMS. Beam 1 (see figure 11) has a Gaussian spatial profile and flat-top temporal shape (pulse duration $\sim 120\text{ps}$). All other beams have top-hat spatial profiles. Beam 2 also has a flat-top temporal shape, while the high energy beams 3 and 4 have near-Gaussian temporal profiles ($\sim 90\text{ps}$ FWHM). Vacuum-based relay telescopes are used throughout the system to relay image the laser rods onto the nonlinear crystals, ensuring the smooth spatial profiles and long-term stability of beam positions.

The stretched broadband seed pulses are amplified in four amplification stages, each consisting of two nonlinear crystals. The configuration of the amplification stages and their efficiencies are summarized in table 4. Wedged crystals, paired with fused silica wedges designed to compensate their angular dispersion, are used throughout the system to avoid the amplification of back-reflections during the relatively long pump pulses.

After the final amplification stage, the signal beam is expanded to 70mm in diameter ($1/e^2$), bounced off a deformable mirror, and sent to a precompressor consisting of 25cm of SF57 glass and 15cm of fused silica (FS). Final compression is performed with 8 chirped mirrors with positive GDD, placed in a vacuum chamber to avoid self-focusing in air. The aperture of all compressor optics is 100mm . The total throughput is 83%, including the gold-coated deformable mirror and a 4% reflection from one surface of the FS blocks, which is deliberately left uncoated to produce a relatively strong and undistorted reflection used for continuous monitoring of system performance. Therefore, the final compressed output energy is 32mJ .

Figure 15 shows the final output spectrum, along with a spectral phase measured using the d-scan [45] technique, as well as the corresponding pulse profile, measured after the optimization of the spectral phase.

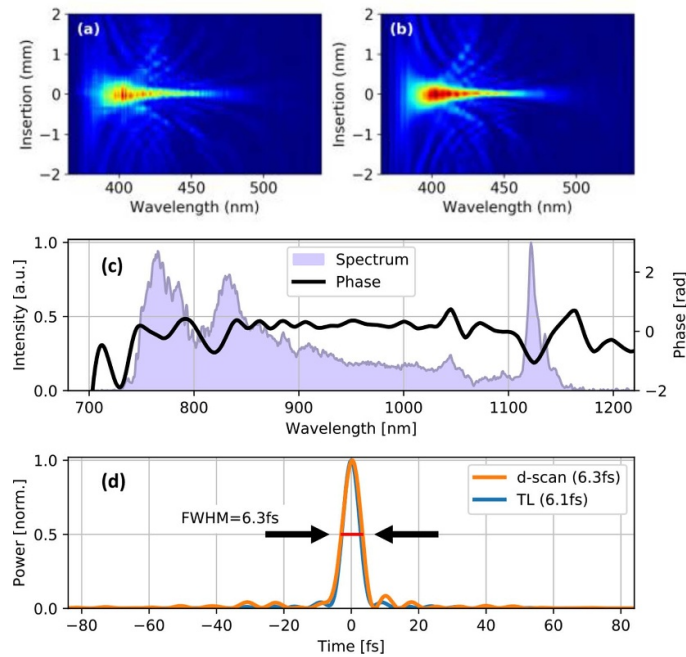


Figure 15. (a) Measured and (b) retrieved d-scan traces. (c) OPCA output spectrum and spectral phase, extracted from the d-scan measurement; (d) corresponding temporal profile (6.3fs FWHM) and its comparison to the transform-limited profile (6.1fs FWHM).

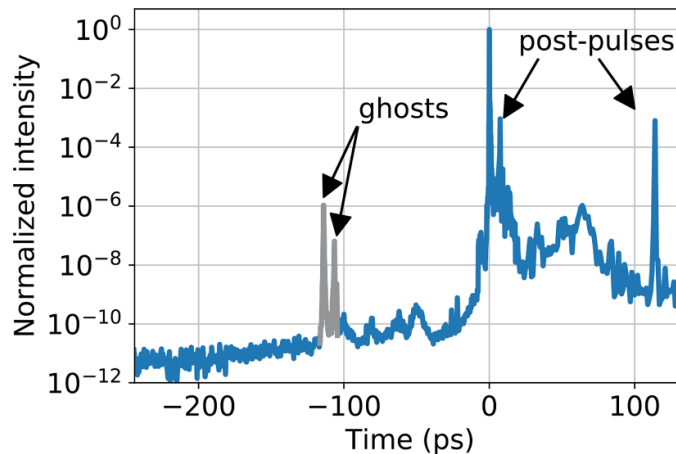
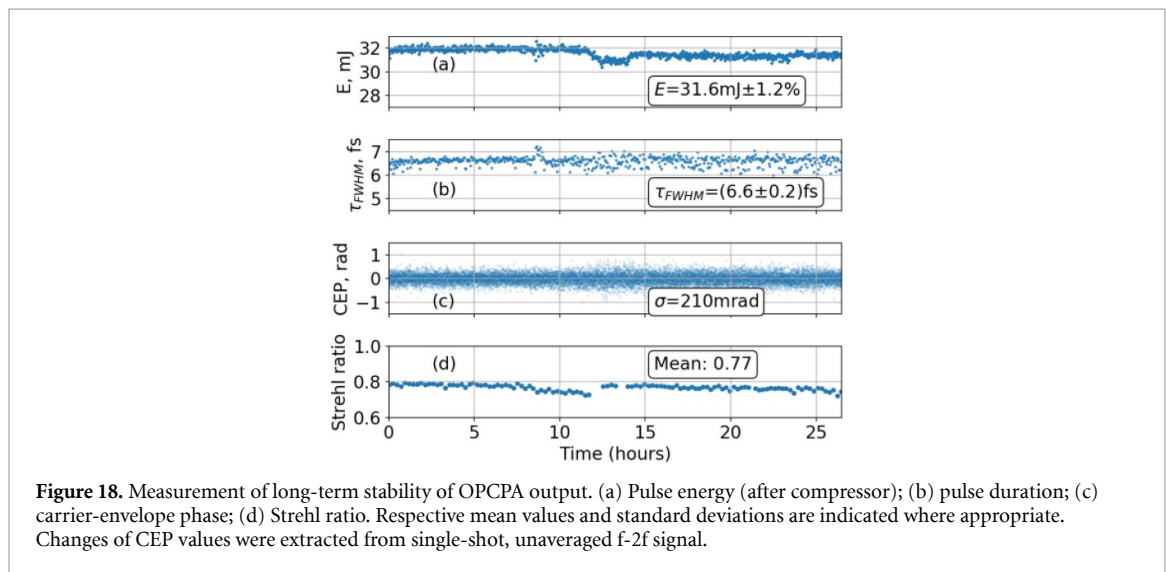
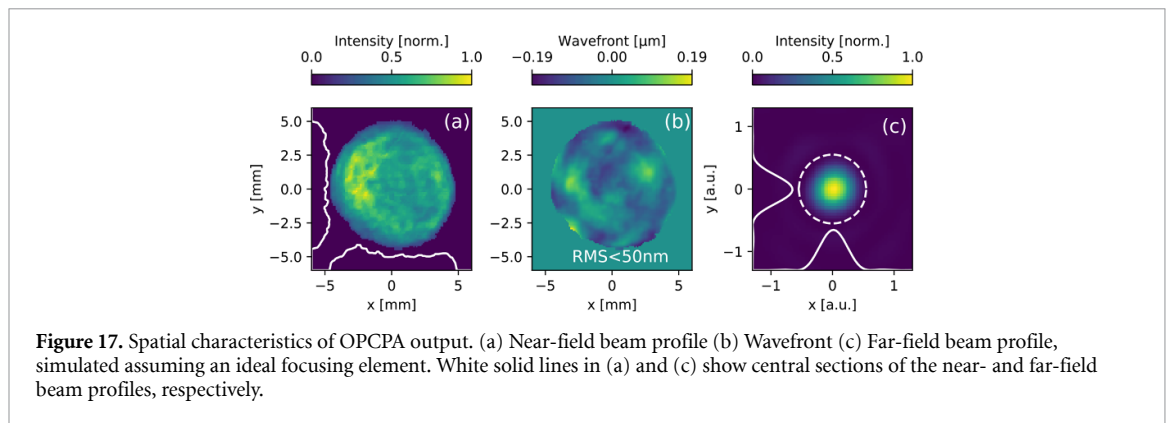


Figure 16. 3rd order autocorrelation measurement of compressed OPCA pulses. Prepulses marked in grey originate from the measurement device.

The d-scan technique was chosen for pulse characterization as it covers the bandwidth which extends over 1100nm. The measured 6.3fs pulse duration corresponds to 2.12 optical cycles at the central wavelength of 891nm.

Due to the intrinsic properties of parametric amplification and the design of the frontend, the pulses also exhibit good signal-to-noise ratio. Prepulse contrast, measured with a high dynamic range 3rd order autocorrelator (Tundra, Ultrafast Innovations), is better than 10^{10} up to 10ps before the main pulse, as seen in figure 16. The pump-seed delays can be adjusted in such a way that almost all of the PSF originating from the OPCA stages pumped by the Nd:YAG laser occurs after and not before the main pulse, which is highly preferable. Furthermore, the 3rd order autocorrelator used for these measurements does not support the full bandwidth of the few-cycle pulses produced by the OPCA, which leads to the underestimation of the intensity of the central peak, and consequently of the measured contrast.

A typical output beam profile is shown in figure 17(a). As M^2 is not a particularly meaningful metric for a hyper-Gaussian beam, the Strehl ratio was used as the beam quality metric instead. The Strehl ratio was evaluated by measuring the wavefront with a Shack-Hartmann type sensor. The wavefront sensor and the deformable mirror were connected by a feedback loop to correct the measured wavefront distortions. As



shown in figure 17(b), the best achieved residual wavefront error is <50nm RMS, which corresponds to a Strehl ratio of 0.9. The typical average Strehl ratio ranges from 0.75 to 0.85. A focal spot, simulated using the measured beam profile and wavefront and assuming an ideal focusing element, is shown in figure 17(c). The central maximum, marked by the dashed white line, contains 80% of all energy, while the intensity level of the faint rings surrounding the central peak is <2%.

3.2. Long-term performance test results

A 24-hour test run was conducted to verify the stability of the final output parameters. During the test run, the following parameters were measured: pulse energy and its stability; beam pointing stability; CEP stability; pulse duration; Strehl ratio. The results are shown in figure 18.

It can be seen that all parameters are maintained with high stability over the extended operation period. It has to be noted that the energy stability is 1.2% over the 24-hour long-term measurement period and it stays below 0.72% over 10min of measurement periods. To achieve this, feedback loops were operated continuously to stabilize the CEP, beam pointing before and after amplification stages, and delay between the frontend and picosecond pump laser. The wavefront was corrected before the measurement, and the feedback loop was then turned off. One extra wavefront correction was necessary after 12h of operation, but other than that, no manual intervention was performed. The spectral phase was also corrected before the measurement, and no corrections to the AOPDF (except for the CEP) were applied during the run.

Overall, the OPCPA produces up to 32mJ pulses at 1kHz repetition rate with <2.3-cycle pulse duration, corresponding to a peak power of 4.8 TW (calculated using the actual pulse profile). Despite the combination of high peak and average power, the high stability of the output parameters, including a CEP noise of 210mrad, can be maintained for >24h.

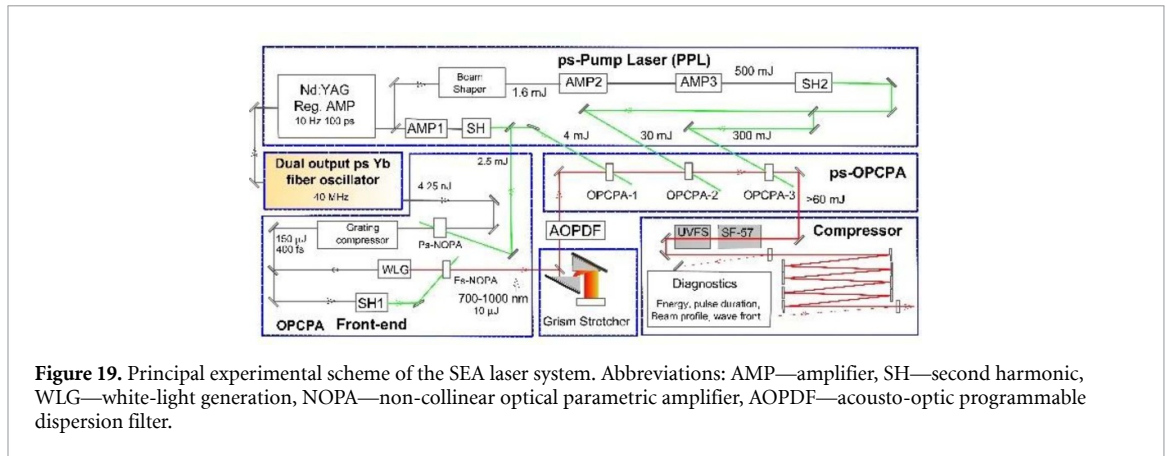


Figure 19. Principal experimental scheme of the SEA laser system. Abbreviations: AMP—amplifier, SH—second harmonic, WL—white-light generation, NOPA—non-collinear optical parametric amplifier, AOPDF—acousto-optic programmable dispersion filter.

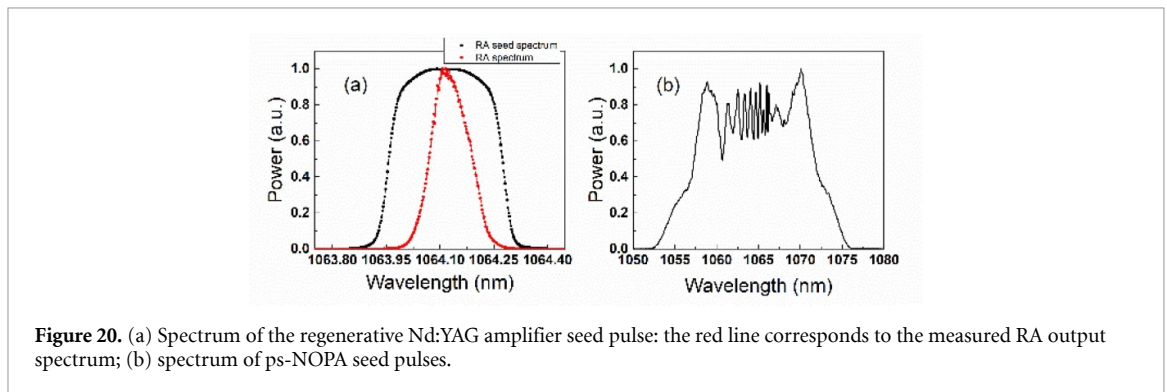


Figure 20. (a) Spectrum of the regenerative Nd:YAG amplifier seed pulse: the red line corresponds to the measured RA output spectrum; (b) spectrum of ps-NOPA seed pulses.

4. SYLOS experimental alignment laser

4.1. Description of the system

As the SYLOS 2 system was expected to be in high demand from external users, there was a need for a backup laser to be used in parallel with the main beam for preparatory purposes. The SYLOS Experimental Alignment (SEA) laser, developed by EKSPLA, can deliver similar pulse parameters at a lower repetition rate.

The principal scheme of the SEA laser is presented in figure 19. This system is based on a unique OPCPA frontend, which uses a single picosecond fibre laser for seeding a diode-pumped solid-state regenerative amplifier (RA) and a white-light supercontinuum generator. This approach eliminates the need for active seed and pump pulse synchronization, and hence significantly simplifies the system. The OPCPA frontend is amplified by femtosecond pulses and then seeds subsequent cascaded picosecond OPCPA stages. Negatively chirped parametric amplification was realized by using a grating-prism pulse stretcher, following the same principles used in SYLOS 2. A bulk glass and chirped mirror compressor was constructed to compensate for system dispersion. Pulse phase fine-tuning [46] was performed by incorporating an AOPDF (Dazzler, Fastlite).

The seed source of the ps-pump system (PPL) and the OPCPA frontend was all-in-fibre picosecond laser which is pictured and described in detail in [47]. A passively mode-locked fibre oscillator generated 2 ps transform-limited pulses at 1064 nm wavelength. The pulse duration and central wavelength were determined by the complex reflectivity profile of chirped fibre Bragg grating (CFBG). A stable mode-locking regime at 40 MHz repetition rate was achieved using a semiconductor saturable absorber mirror (SESAM) as the end mirror of the resonator. Active repetition rate stabilization was realized using a piezo element and temperature tuning, which enabled synchronization to an external clock with a less than 1 ps RMS timing jitter.

Ultrafast radiation from the oscillator was amplified in a Yb³⁺ doped fibre amplifier and divided into two parts. In the first part, pulses were stretched to ~300 ps in duration by a narrowband CFBG. A double thermo-electric controller (TEC) unit was used to adjust the central wavelength of CFBG in order to match seed spectrum to the gain maximum of Nd:YAG RA (figure 20(a)). A temperature gradient was created to change the dispersion of CFBG and consequently to tune and set the desired pump pulse duration. Stretched pulses were amplified in Nd:YAG RA and then in double-pass Nd:YAG amplifiers (described below). The spectral bandwidth and duration of the amplified chirped pulses were approximately one third of that of the input pulse due to the gain narrowing effect.

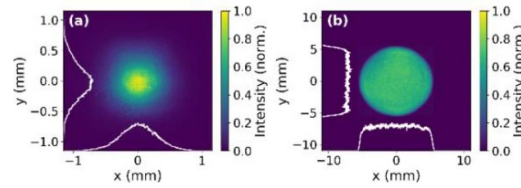


Figure 21. PPL second harmonic beam intensity distributions: (a) a 4mJ SH1 beam profile at the OPCPA-1 crystal plane; (b) a 300mJ SH2 beam profile at the OPCPA-3 crystal plane.

The second part of the fibre laser was used for femtosecond seed formation (Fs-NOPA seed). At first, pulses were amplified to 3nJ energy in a Yb^{3+} doped fibre amplifier. Then the pulse spectrum was broadened to $\sim 15\text{nm}$ by self-phase modulation (SPM) in a single-mode fibre (figure 20(b)). After that, pulses were stretched to $\sim 120\text{ps}$ by a broadband CFBG, which was designed to ensure that the cumulative second and third order dispersion of the CFBG and of the nonlinear fibre was compensated by the grating compressor to achieve a shorter pulse duration and better contrast. Finally, pulses were amplified again in another fibre amplifier up to 4.25nJ and directed to a picosecond noncollinear optical parametric amplifier (Ps-NOPA). A 9mm long, type I BBO Ps-NOPA crystal was pumped using a part (2.5mJ) of the frequency doubled pulses originating from the diode pumped Nd:YAG amplifier (AMP1). Pulses of $200\mu\text{J}$ were produced with an 8% energy conversion efficiency. After the Ps-NOPA stage, pulses were compressed down to 400fs in a Treacy-type diffraction grating compressor [48], which was constructed by using 1600groovesmm – transmission gratings working in Littrow configuration. The efficiency of the compressor was $\sim 75\%$.

A small fraction of the parametrically amplified and compressed pulses were focused on a 5mm thick sapphire plate to generate white-light (WLG in figure 19.). The pulse energy and focusing conditions were optimized to produce smooth and stable supercontinuum. The remaining energy ($\sim 150\mu\text{J}$) was frequency doubled in a 1.5mm long BBO crystal and used as a pump for the femtosecond NOPA (Fs-NOPA). Parametric amplification was realized in a 2mm long, type I BBO crystal at a phase-matching angle of 24° and at a noncollinear angle of $\sim 2.4^\circ$ to achieve the broadest amplification bandwidth. An approximately 11% pump-to-signal energy conversion efficiency was achieved at $\sim 150\text{GWcm}^{-2}$ pump intensity, resulting in $10\mu\text{J}$ broadband pulses. The parametrically amplified pulse spectrum spans from 700nm to 1000nm, which corresponds to a less than 10fs Fourier transform-limited pulse duration.

After the Fs-NOPA stage, broadband pulses were stretched to $\sim 60\text{ps}$ in a negative dispersion grating-prism stretcher and AOPDF. The stretched pulses after ‘Dazzler’ were directed to the ps-OPCPA part for further parametric amplification by using the output of the picosecond pump laser.

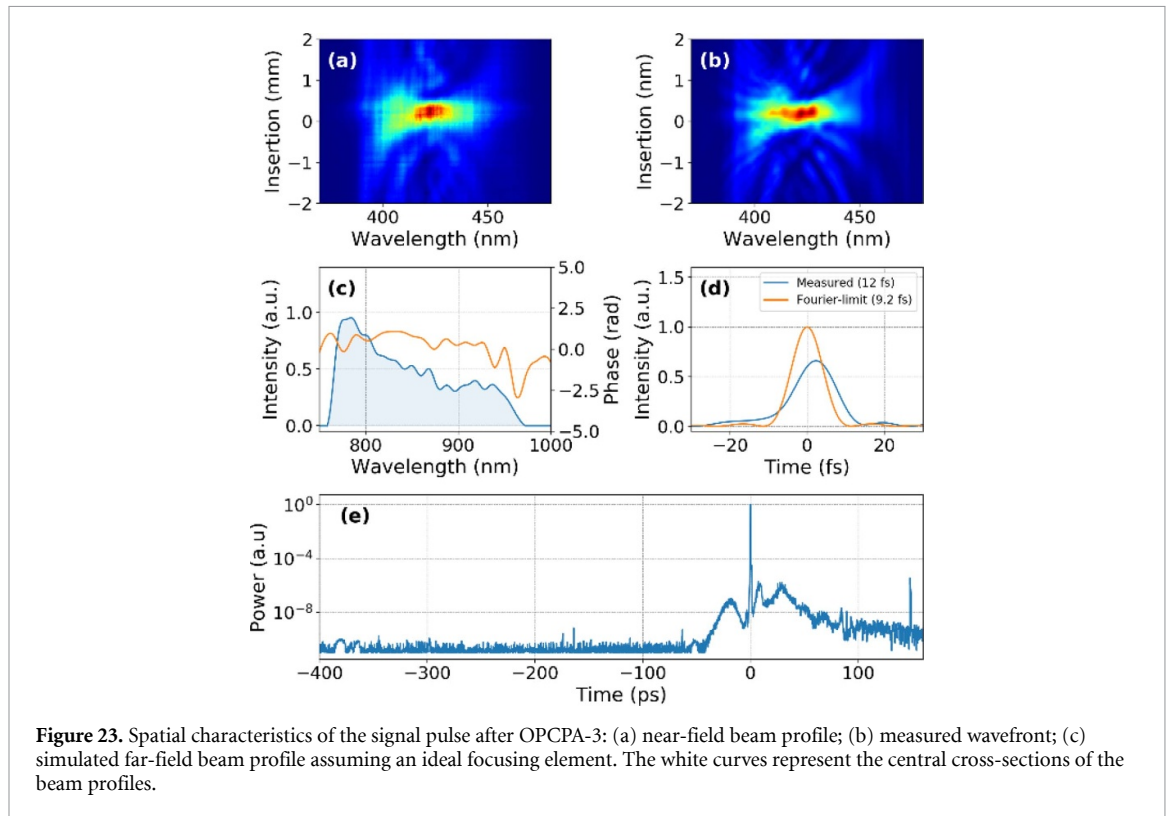
The second harmonic (SH) of the PPL was used to pump both μJ output level OPCPA frontend (described above) and multi-mJ output ps-OPCPA stages. The diode pumped RA and the double-pass amplifier AMP1 ensured excellent energy and beam pointing stability, which was critical for the low energy OPCPA frontend and the OPCPA-1 stage, while flash-lamp pumped amplifiers AMP2 and AMP3 were used as a cost-effective and well developed technique to boost energy to the sub-Joule level and pump the OPCPA-2 and OPCPA-3 stages.

This hybrid concept was realized by dividing a 4mJ pulse energy ($\sim 0.15\%$ RMS) RA output into two parts. The lower (0.7mJ) energy part was amplified in a diode pumped ($\text{Ø}5 \times 50\text{mm}$ Nd:YAG) amplifier module (AMP1) up to 12mJ ($\approx 0.2\%$ RMS) and frequency doubled in a type I LBO crystal (SH1), providing 7mJ ($\approx 0.25\%$ RMS) second harmonic pulses at 532nm wavelength. Part of the SH1 energy (2.5mJ) was used for pumping the OPCPA frontend while the residual 4mJ pulses were directed to pump the OPCPA-1 stage, where $< 1\mu\text{J}$ energy, broadband NIR radiation was amplified in a 9mm long BBO crystal up to $240\mu\text{J}$. The beam profile of the pump is depicted in figure 21(a).

The high energy ($\approx 3.2\text{mJ}$) RA output radiation was amplified in AMP2 and AMP3, providing pump beams for the final OPCPA 2 and 3 stages. The pump beam profile is one of the most critical issues in high energy OPCPA. Knowing that the top-hat beam profile (super-Gaussian distribution) is the best solution for the pump [49], we implemented a beam shaping system using the serrated pattern aperture technique [50, 51]. It has to be noted that in SYLOS 2 different beam shaping approach is used due to the hundred times higher average power. The serrated aperture plane was subsequently relay imaged to laser amplifiers (AMP2 and AMP3), the second harmonic generator (SH2) and to the OPCPA 2 and 3 stages. In the flash-lamp pumped amplifier AMP2 ($\text{Ø} 8 \times 85\text{mm}$ Nd:YAG), 90ps duration pulses were amplified from 1.6mJ to $\approx 110\text{mJ}$ energy. In the next stage (AMP3, $\text{Ø} 12 \times 85\text{mm}$ Nd:YAG), the OPCPA pump pulse energy was boosted up to $\approx 500\text{mJ}$ and frequency doubled in SH2 (6mm long, type I LBO) with a 67% conversion

Table 5. Parameters of the ps-OPCPA stages of the SEA laser.

OPCPA	Pump energy (mJ)	Pump intensity (GWcm^{-2})	Signal pulse energy (mJ)	Signal pulse energy stability RMS (%)	BBO thickness (mm)	Pump-to-signal conversion efficiency (%)
Seed	—	—	0.0001	1.9	—	—
1	4	7.4	0.24	0.7	9	6
2	30	2	5	0.8	5	16
3	300	3.7	62	0.95	3	19



efficiency. Pump pulse energy stability was $\sim 0.5\%$ RMS, measured from 300 consecutive shots. The shaped PPL SH2 output beam could be approximated by the 11th order hyper-Gaussian function (figure 21(b)).

The SH2 output beam was split into two: $\approx 30\text{mJ}$ for the OPCPA-2 stage and $\approx 300\text{mJ}$ for the OPCPA-3 stage pumping 5mm and 3mm long BBO nonlinear crystals, respectively. For all OPCPA stages, Type 1 phase-matching and an internal noncollinear angle of ≈ 2.40 was chosen. Parameters of the ps-OPCPA stages are summarized in table 5. The energy of the amplified signal pulse after OPCPA-3 is 62 mJ and the beam profile is presented in figure 23(a).

The parametrically amplified beam was expanded to a diameter of $\approx 80\text{mm}$ ($1/e^2$ max. intensity level) and was reflected to the bulk glass compressor, consisting of a 350mm long SF-57 and a 100mm long fused silica glass sheets. The final pulse compression down to 12 fs was achieved in a 8-bounce positive chirp ($\text{GDD} \approx 100 \text{ fs}^2$ per reflection) mirror compressor. Pulse duration measurements (d-scan technique), and temporal contrast characterization ('Sequoia', Amplitude Technologies) are provided in figure 22.

The overall compressor transmission was $\approx 70\%$, which corresponded to an output pulse energy of 42.5mJ. The efficiency of the compressor system is quite modest due to the use of two uncoated UVFS wedged windows producing beam samples to the diagnostic system. If we disregard these reflection losses, the compressor transmission could be improved up to 80%.

The maximum measured prepulse amplified parametric fluorescence intensity value was 10^{-7} with respect to the main pulse. The pulse contrast value was already limited by the noise level of the measuring device (5×10^{-11}) 50ps before the main pulse.

An active wavefront correction system (Imagine Optics) consisting of a deformable mirror (ILAO star) and a Shack-Hartmann sensor (HASO4-First) was implemented in the system to correct for aberrations caused by the magnifying telescope and the surface imperfections of optical elements. This way the best

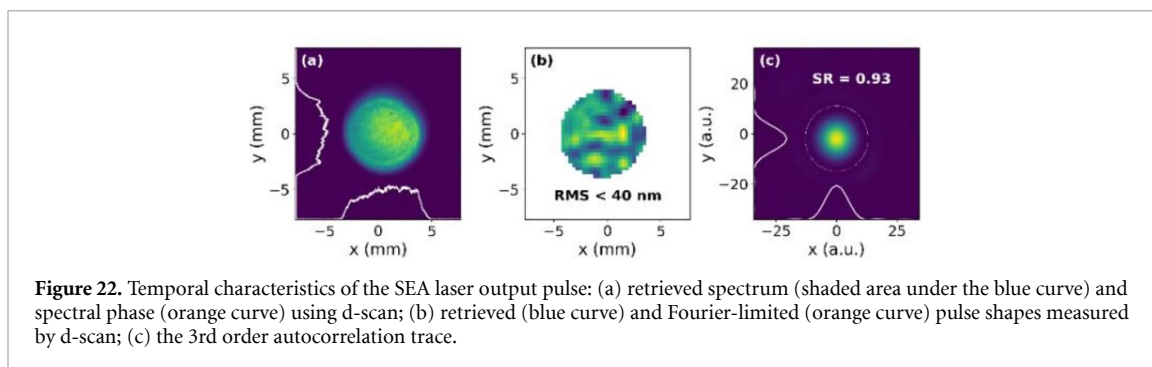


Figure 22. Temporal characteristics of the SEA laser output pulse: (a) retrieved spectrum (shaded area under the blue curve) and spectral phase (orange curve) using d-scan; (b) retrieved (blue curve) and Fourier-limited (orange curve) pulse shapes measured by d-scan; (c) the 3rd order autocorrelation trace.

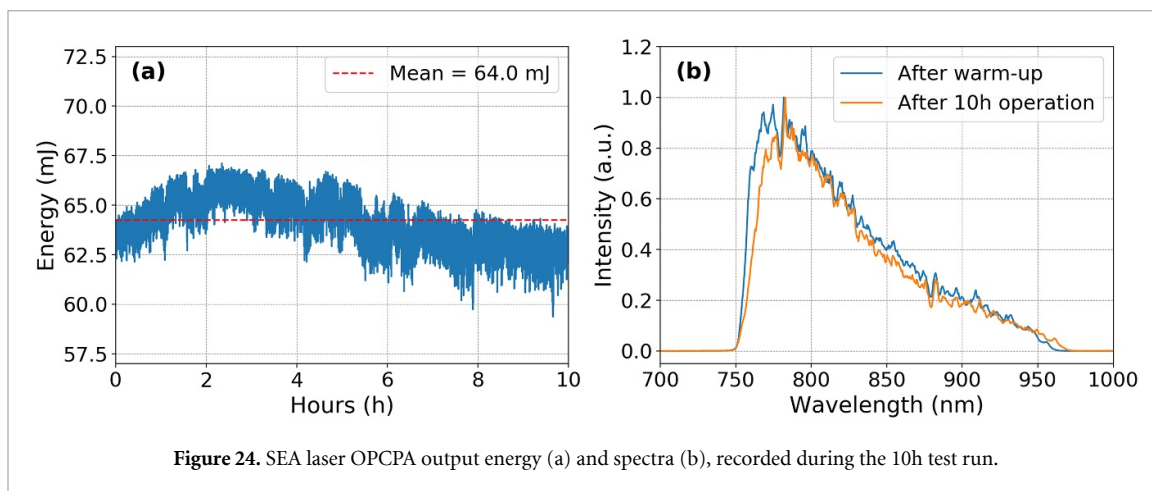


Figure 24. SEA laser OPCPA output energy (a) and spectra (b), recorded during the 10h test run.

achieved wavefront error was $<40\text{nm}$ RMS (figure 23(b)), which corresponds to a Strehl ratio value of 0.93 (figure 23(c)). The encircled area in figure 23(c) contains $>85\%$ of the total energy.

4.2. Long-term performance test results

In order to verify the long-term stability of SEA laser system, key output parameters including OPCPA output pulse energy and spectrum were logged for 10h uninterrupted operation starting from 20min warm up time period. The energy stability graph in figure 24(a) shows a 4% output energy drift with respect to the mean value. Central wavelength of the output pulse spectrum (calculated by using the power-weighted mean) shifted from 825nm to 830nm during the long-term test (figure 24(b)).

Note that during the test run, none of the energy and beam stabilization feedback loops was applied, hence pulse energy and spectrum drift values could be considered as modest. We determined that adjustment of the motorized pump-signal delay line in a range of 10 ps was sufficient for the recorded energy drift compensation.

5. Summary and outlook

In this paper, we presented the SYLOS 2 and SEA lasers of ELI-ALPS. The schematics, specifications and long-term performance test results of these systems are discussed in details, together with a numerical study of the broadband OPCPA schemes.

Two broadband OPCPA schemes were examined numerically: single LBO crystal in noncollinear geometry and spectral multiplexing in the double BBO configuration. According to the theoretical study, when pumped at 10GWcm^{-2} level, an LBO can amplify over a broad wavelength range, from 750nm to 1200nm. However, the gain at longer wavelengths and the pump-to-signal conversion efficiency decrease in the power amplifier stages where the pump intensity is lower due to safety reasons.

Spectral multiplexing in the double BBO configuration is a simple and compact design which can efficiently amplify over almost one octave spectral width necessary to reach the two-cycle pulse duration. However, this configuration introduces strong spatiotemporal couplings in case of small beam sizes caused by lateral walk-off and it is therefore applicable only in the power amplifier stages.

We can conclude that the numerical simulations were extremely useful in selection of the OPCPA crystal parameters. There are, however, few differences between the simulated and experimentally realized OPCPA stages, particularly in the 2nd OPCPA stage. In the simulations, a single LBO crystal was found to be

Table 6. Measured output parameters of SYLOS 2 and SEA systems.

	Mean energy (mJ)	Energy stability RMS (%)	Duration (fs)	Peak power (TW)	CEP (mrad)	Strehl ratio	Central wavelength (nm)	Warm-up time (min)
SYLOS 2	32	1.2	6.6	4.8	210	0.77	891	45
SEA	42.5	0.87	12	3.2	–	0.93	825	20

sufficient for reaching the required efficiency and bandwidth, which is necessary for the power amplifier stages. However, in the experimental realization, the single LBO crystal was unable to amplify the long wavelength side of the spectrum efficiently. Consequently, this layout was modified and the 730–1000nm and 1000–1150nm part of the spectrum was multiplexed using BBO and LBO crystals, respectively. This difference is responsible mostly for the deviation between the simulated and experimentally measured spectral shape.

The SYLOS 2 system produces CEP-stable, 4.8 TW, <2.3 cycle pulses at 1kHz repetition rate on a daily basis. The system consists of a stable frontend, which produces passively CEP-stabilized, background-free (low-PSF, pre- and postpulse free) pulses for seeding ps-OPCPA stages pumped by a diode pumped solid-state laser. The reliability of the system was demonstrated by a 24h test run, during which energy, pulse duration, CEP-stability and the Strehl ratio were continuously measured. The results are summarized in table 6. The SEA laser produces 3.2 TW, 12fs pulses at 10Hz repetition rate. The system consists of a fibre laser seeded OPCPA frontend, a hybrid (diode and flash-lamp pumped) picosecond Nd:YAG laser, which is also seeded by the fibre laser, and the three-stage ps-OPCPA unit. The reliability of this system was demonstrated by a 10h test run. During this period, the output energy and the spectrum were measured continuously, while the pulse duration and Strehl ratio were measured after the warm-up time. These results are also summarized in table 6.

These laser systems are to drive several beamlines at the ELI-ALPS user facility, including gas-phase and solid surface-based high harmonic generation stations producing attosecond light sources. In addition, electron and ion acceleration beamlines are also under implementation, aiming at applications from radiobiology through material sciences to nuclear physics.

Simulation results also suggests that multiple crystal configurations are able to support even shorter pulse durations and higher pulse energies. In practice, limiting factors for the pulse duration is mainly the complexity of the arrangement, which could make other solutions more attractive. Pulse energy, however, only limited by the crystal sizes and pump power. We will continue the development of the 1kHz SYLOS laser in these two directions in parallel. The first direction aims at pulse shortening to near single cycle using post-compression techniques, whereas several different solutions show promising advancements, such as the hollow-core fiber technology or the multiple thin plate approach. The second direction will scale up the pulse energy to 100mJ with the implementation of further similar ps pump systems and OPCPA stages.

Acknowledgments

The ELI-ALPS project (GINOP-2.3.6-15-2015-00001) is supported by the European Union and co-financed by the European Regional Development Fund. We thank Dr. Alexey Andrianov for assistance with the numerical OPCPA code.

ORCID iD

S Toth  <https://orcid.org/0000-0002-8516-3962>

References

- [1] Sansone G *et al* 2006 *Science* **314** 443
- [2] Chini M, Zhao K and Chang Z 2014 *Nat. Photon.* **8** 178
- [3] Gilbertson S, Wu Y, Khan S D, Chini M, Zhao K, Feng X and Chang Z 2010 *Phys. Rev. A* **81** 043810
- [4] Mondal S *et al* 2018 *J. Opt. Soc. Am. B* **35** A93
- [5] Goulielmakis E *et al* 2008 *Science* **320** 1614
- [6] Beaulieu B, Lifschitz A and Faure J 2014 *New J. Phys.* **16** 023023
- [7] Irvine S E, Dombi P, Farkas G and Elezabi A Y 2006 *Phys. Rev. Lett.* **97** 146801
- [8] Zherebtsov S *et al* 2011 *Nat. Phys.* **7** 656
- [9] Nerush E N and Kostyukov I Y 2009 *Phys. Rev. Lett.* **103** 035001
- [10] Rác P, Irvine S E, Lenner M, Mitrofanov A, Baltuska A, Elezabi A Y and Dombi P 2011 *Appl. Phys. Lett.* **98** 111116

- [11] Yamakawa K, Aoyama M, Matsuoka S, Kase T, Akahane Y and Takuma H 1998 *Opt. Lett.* **23** 1468
- [12] Yu T J, Lee S K, Sung J H, Yoon J W, Jeong T M and Lee J 2012 *Opt. Express* **20** 10807
- [13] Eilanlou A A, Nabekawa Y, Ishikawa K L, Takahashi H and Midorikawa K 2008 *Opt. Express* **16** 13431
- [14] Kalashnikov M, Cao H, Osvay K and Chvykov V 2016 *Opt. Lett.* **41** 25
- [15] Cavalieri A L et al 2007 *New J. Phys.* **9** 242
- [16] Böhle F et al 2014 *Laser Phys. Lett.* **11** 095401
- [17] Hadrich S et al 2016 *Opt. Lett.* **41** 4332
- [18] Ueffing M, Reiger S, Kaumanns M, Pervak V, Trubetskov M, Nubbemeyer T and Krausz F 2018 *Opt. Lett.* **43** 2070
- [19] Hauri C P, Schlup P, Arisholm G, Biegert J and Keller U 2004 *Opt. Lett.* **29** 1369
- [20] Zapata L E et al 2015 *Opt. Lett.* **40** 2610
- [21] Müller M et al 2016 *Opt. Lett.* **41** 3439
- [22] Michailovas K, Baltuska A, Pugzlys A, Smilgevicius V, Michailovas A, Zaukevičius A, Danilevičius R, Frankinas S and Rusteika N 2016 *Opt. Express* **24** 22261
- [23] Fattahi H, Alismail A, Wang H, Brons J, Pronin O, Buberl T, Vámos L, Arisholm G, Azzeer A M and Krausz F 2016 *Opt. Lett.* **41** 1126
- [24] Zapata L E, Reichert F, Hemmer M and Kärtner F X 2016 *Opt. Lett.* **41** 492
- [25] Schulz M et al 2011 *Opt. Lett.* **36** 2456
- [26] Nubbemeyer T et al 2017 *Opt. Lett.* **42** 1381
- [27] Klingebiel S, Wandt C, Skrobol C, Ahmad I, Trushin S A, Major Z, Krausz F and Karsch S 2011 *Opt. Express* **19** 5357
- [28] Wandt C et al 2014 *Laser Photonics Rev.* **8** 875
- [29] Rivas D E et al 2017 *Sci. Rep.* **7** 5224
- [30] Herrmann D, Veisz L, Tautz R, Tavella F, Schmid K, Pervak V and Krausz F 2009 *Opt. Lett.* **34** 2459
- [31] Witte S, Zinkstok R T, Wolf A L, Hogervorst W, Ubachs W and Eikema K S E 2006 *Opt. Express* **14** 8168
- [32] Kessel A et al 2018 *Optica* **5** 434
- [33] Adachi S, Ishii N, Kanai T, Kosuge A, Itatani J, Kobayashi Y, Yoshitomi D, Torizuka K and Watanabe S 2008 *Opt. Express* **16** 14341
- [34] Fattahi H et al 2014 *Optica* **1** 45
- [35] Prinz S et al 2018 *Opt. Express* **26** 1108
- [36] Federico J A F, Tobias W, Mikhail O, Felix S, Claus P S and Marc J J V 2019 Short-pulse high-energy lasers and ultrafast optical technologies *Proc. SPIE* vol 11034 p 1103401
- [37] Budriunas R, Stanislauskas T, Adamonis J, Aleknavicius A, Veitas G, Gadonas D, Balickas S, Michailovas A and Varanavicius A 2017 *Opt. Express* **25** 5797
- [38] Baudisch M, Pires H, Ishizuki H, Taira T, Hemmer M and Biegert J 2015 *J. Opt.* **17** 094002
- [39] Herrmann D, Homann C, Tautz R, Scharrer M, Russell P S J, Krausz F, Veisz L and Riedle E 2010 *Opt. Express* **18** 18752
- [40] Veisz L, et al 2013 *Conf. Lasers and Electro-Optics Pacific Rim* p TuD2-3
- [41] Andrianov A, Szabo A, Sergeev A, Kim A, Chvykov V and Kalashnikov M 2016 *Opt. Express* **24** 25974
- [42] Cerullo G and Silvestri S D 2003 *Rev. Sci. Instrum.* **74** 1
- [43] Baltuska A, Fuji T and Kobayashi T 2002 *Phys. Rev. Lett.* **88** 133901
- [44] Dou T H, Tautz R, Gu X, Marcus G, Feuer T, Krausz F and Veisz L 2010 *Opt. Express* **18** 27900
- [45] Miranda M, Arnold C L, Fordell T, Silva F, Alonso B, Weigand R, L'Huillier A and Crespo H 2012 *Opt. Express* **20** 18732
- [46] Lorient V, Gitzinger G and Forget N 2013 *Opt. Express* **21** 24879
- [47] Danilevičius R, Zaukevičius A, Michailovas A and Rusteika N 2016 *Opt. Express* **24** 17532
- [48] Treacy E 1969 *IEEE J. Quantum Electron.* **5** 454
- [49] Bagnoud V, Begishev I A, Guardalben M J, Puth J and Zuegel J D 2005 *Opt. Lett.* **30** 1843
- [50] Auerbach J M and Karpenko V P 1994 *Appl. Opt.* **33** 3179
- [51] Adamonis J, Antipenkov R, Kolenda J, Michailovas A, Piskarskas A P and Varanavicius A 2012 *Quantum Electron.* **42** 567